Thermal and Fluid Analysis of a Low-Bypass Turbofan Engine

Satvik Mishra Ansh Bansal Aman Vats
Department of Mechanical, Production & Industrial and Automotive Engineering
Delhi Technological University, Delhi, India

Abstract— Low-bypass turbofan engines play a central role in aircraft propulsion: they generate thrust both from the cooler bypass stream and the hot core jet, which lets them remain efficient over a wide span of flight regimes. Predicting their behaviour accurately is, however, far from straightforward, since thermodynamic energy conversion, compressible-flow effects, and component-level losses are strongly coupled. This paper develops a physics-based numerical framework for the thermal and fluid evaluation of such an engine. The cycle is built on steady-flow relations derived from the first and second laws of thermodynamics together with the relevant energy-transfer equations. The engine is treated as a sequence of control volumes — intake, compressor, combustor, turbine, and nozzle — so that performance can be evaluated under different operating conditions. MATLAB is used to numerically solve the governing equations and iterate over key design variables. Outputs include specific thrust, thrust-specific fuel consumption (TSFC), propulsive efficiency, fuel-to-air ratio, and station-wise entropy generation. A simplified three-dimensional geometry is constructed in SolidWorks to define the surface boundaries, while CFD and thermal simulations are run in SimScale to capture local flow and temperature behaviour. The combined results provide a structured framework that links thermodynamic, geometric and numerical analysis, and they highlight the trade-offs between specific thrust, propulsive efficiency, and irreversibility as the bypass ratio is varied.

Keywords—Low-bypass turbofan; thermodynamic cycle; computational fluid dynamics (CFD); specific thrust; propulsive efficiency; entropy generation; MATLAB; SolidWorks.

I. INTRODUCTION

Aircraft propulsion has progressed remarkably since the earliest jet engines. Today the turbofan is the dominant choice for both commercial and military platforms. The low-bypass variant occupies a particularly important niche because it merges the high-speed capability of a turbojet with the better fuel economy that bypass flow brings. A portion of the inlet air is routed through an annular duct around the combustion core, generating an additional low-velocity thrust component alongside the high-temperature core jet. The outcome is a propulsion architecture well suited to transonic and supersonic flight, where pure turbojets become thermodynamically wasteful and high-bypass designs suffer from large nacelle drag.

In spite of how widely they are used, accurately predicting turbofan behaviour remains challenging. Performance arises from a tightly coupled interplay between compressible flow, thermodynamic energy transfer, heat-transfer effects, and component-level irreversibilities. Conventional Brayton-cycle treatments are useful for global metrics but cannot resolve the spatial flow features, local pressure losses, or wall-temperature gradients that dictate real component behaviour. Fully resolved three-dimensional CFD can capture these effects but is computationally expensive at the conceptual stage. The present work is driven by this contrast: a middle path is required that goes beyond ideal-cycle assumptions yet avoids the cost of fully resolved unsteady simulation.

The framework proposed here couples MATLAB-based cycle modelling, SolidWorks three-dimensional geometric modelling, and CFD/thermal simulation in SimScale. The engine is decomposed into control volumes — intake, fan, compressor, combustor, turbine, afterburner and nozzle — each of which obeys steady-flow energy and mass conservation. Real-world effects such as component efficiencies, pressure losses, and high-altitude ambient conditions are explicitly included.

A. Scope and Approach

The scope covers (i) a steady-flow thermodynamic model that captures every major component; (ii) a MATLAB implementation that performs parametric sweeps over bypass ratio and other design variables; (iii) a three-dimensional CAD model of the engine and its subsystems; and (iv) CFD and thermal simulation for local flow-field and temperature characterisation. The combination is meant to provide predictions that are physically more realistic than pure cycle analysis while remaining far cheaper than full unsteady three-dimensional CFD.

B. Organisation of the Paper

Section II reviews the literature on turbofan modelling, CFD, exergy assessment, combustion optimisation, and alternative-fuel studies. Section III highlights the gaps that motivate this study. Section IV lists the objectives, while Section V describes the methodology. Section VI presents the numerical and simulation results. Section VII gives representative excerpts of the MATLAB code. Section VIII summarises the conclusions and Section IX outlines possible extensions.

II. LITERATURE REVIEW

A substantial body of work exists on the analysis and design of turbofan engines. The literature spans thermodynamic cycle studies, CFD-based flow analyses, combustion-chamber

design, exergy and sustainability assessments, and investigations of alternative fuels and hybrid propulsion. Only the most directly relevant contributions are summarised below; the complete reference list appears at the end of the paper.

A. Thermodynamic and Cycle Studies

Liew, Urip and Yang [1]–[3] carried out detailed on-design and off-design analyses of two-spool separate-exhaust turbofans equipped with an interstage turbine burner (ITB), and concluded that the ITB can substantially raise specific thrust and thermal efficiency while keeping the required turbine inlet temperature within acceptable bounds. Tai et al. [4] used genetic-algorithm optimisation to identify design points that maximise both energy and exergy efficiency of a two-spool engine subject to multiple constraints. Sabzehali, Farahani and Mosavi [5] examined a hydrogen-fuelled turbofan and reported notable improvements in overall efficiency together with significant reductions in CO_2 emissions when Jet-A is replaced by hydrogen. Yadav [6] presented a thermodynamic study showing that the Mach number at which propulsive efficiency peaks moves toward higher bypass ratios as flight Mach number falls.

B. Multi-Fidelity and Simulation Studies

Turner, Reed and Ryder [7] introduced a multi-fidelity simulation in which a zero-dimensional cycle code is coupled with higher-fidelity component models. Magrini and Benini [29] extended this idea to engines with variable-area nozzles using two- and three-dimensional CFD, and showed that installation effects and nacelle drag substantially modify propulsive behaviour. Lytle [17] described the NASA Numerical Propulsion System Simulation (NPSS), emphasising the role of object-oriented multi-disciplinary frameworks. Jorgenson, Veres and Coennen [8] examined turbofan response to ice-crystal ingestion, while Veres [9] outlined a mean-line flow analysis method for axial and centrifugal compressors. Abdol-Hamid et al. [10] applied high-fidelity CFD to exhaust-nozzle flows and demonstrated that shock–boundary-layer interactions shift discharge coefficients away from idealised nozzle theory.

C. Combustion, Materials, and Installation Effects

Rizk and Mongia [16] assessed lean low-NOx combustion strategies and quantified the trade-off between lean stability and emission reduction. Clarke, Oechsner and Padture [15] reviewed thermal-barrier coatings, highlighting how advanced coatings make higher turbine inlet temperatures feasible. Barber, Paterson and Skebe [12] investigated forced-mixer lobe flows and demonstrated that careful lobe design can simultaneously improve pressure recovery and reduce noise. Magrini et al. [14] analysed powered-turbofan effects on aircraft aerodynamics under high-lift conditions using the NASA CRM-HL configuration. Mark and Selwyn [30] designed and analysed an annular combustor for a jet-trainer low-bypass engine, achieving roughly 96 % combustion efficiency with an acceptable pattern factor in a short overall length.

D. Supersonic, Variable-Cycle, and Sustainable Concepts

Piccirillo, Gregorio and Fusaro [13] developed a mixed-flow turbofan model aimed at sustainable supersonic platforms. Feng et al. [21] proposed a bypass-driven mixing turbofan (BDMT) combining a rear variable-area bypass injector with a guide-vane bleed ring to extend the operating envelope beyond Mach 4. Zhao, Grönstedt and Kolb [28] evaluated multi-fuel turbofans burning blends of Jet-A and hydrogen, finding that increasing the hydrogen fraction raises thermal efficiency by roughly 1 % and lowers engine dry weight by up to 7 %. Xu et al. [26] tested 100 % HEFA sustainable aviation fuel in a small-scale turbofan and reported reductions in CO, CO_2 and particulate matter of up to 96 % relative to diesel, with only a small NOx penalty.

Ogur et al. [27] performed a five-dimensional analysis (energy, exergy, exergo-economic, exergo-environmental, sustainability) of a GEnx-1B76 engine running on hydrogen and kerosene and showed that hydrogen eliminates CO_2 emissions. Coşkun et al. [24] demonstrated that injecting water into the high-pressure compressor lowers compressor outlet temperature from approximately 885 K to 600 K and increases thrust by up to about 15 %. Balli and Caliskan [22] performed a combined aviation, energy, exergy and environmental study of a JT15D engine and identified the combustor as the component with the largest irreversibility. Najjar [23] showed that inlet-air cooling combined with cogeneration can raise gas-turbine power output by roughly 21 % and thermal efficiency by about 38 %. Xiu et al. [18] and Xu et al. [19] explored hybrid turbofan architectures coupled with fuel cells. Akdeniz, Balli and Caliskan [20] studied dual-fuel turbofan operation, while Pavlenko, Dvirnyk and Przysowa [25] proposed advanced materials — sintered titanium, aluminium alloys and titanium aluminides — for compressor blades of small UAV turbofans.

E. Synthesis

Four recurring conclusions emerge from the literature. First, performance is most sensitive to compressor pressure ratio, turbine inlet temperature, bypass ratio, and component efficiencies. Second, coupling cycle codes with simplified CFD is needed to capture installation-related pressure losses and stream-mixing behaviour that zero-dimensional models miss. Third, hydrogen, sustainable aviation fuels (SAF) and hybrid-electric architectures all promise measurable emission reductions but introduce distinct challenges in combustion stability, structural loading or energy storage that are not yet fully resolved. Fourth, off-design and part-load operation continue to be areas where efficiency degrades significantly.

III. GAP IDENTIFICATION

Several gaps remain. First, very few open-access cycle tools are tailored for military low-bypass or supersonic configurations; most existing codes are either commercial packages or general-purpose tools that have not been calibrated for afterburning. Second, combustor modelling still relies heavily on empirical correlations, and three-dimensional RANS calculations struggle to predict radial temperature profiles, lean-blowout limits, ignition behaviour, and NOx formation within a single framework. Third, blended sustainable aviation

fuels are currently restricted to a 50 % blending cap and their long-term impact on liner durability and combustion stability under altitude conditions is not well understood. Fourth, system-level propulsion efficiency continues to fall at off-design power settings, which account for a substantial fraction of real mission time. The present study addresses a subset of these issues by offering a transparent, physics-based framework — built without commercial licences — that ties together thermodynamic cycle modelling, CAD geometry, and CFD/thermal simulation.

IV. OBJECTIVES OF THE STUDY

The primary aim is to develop an integrated framework for the thermal and fluid analysis of a low-bypass turbofan engine. Specific objectives are: (a) to construct a steady-flow thermodynamic model treating the engine as a sequence of control volumes and applying the first and second laws to each; (b) to implement the model in MATLAB and compute specific thrust, TSFC, propulsive efficiency, exhaust velocities, fuel-to-air ratio, and entropy generation; (c) to perform a parametric study over bypass ratio, compressor pressure ratio, and turbine inlet temperature while accounting for component efficiencies and pressure losses; (d) to carry out a thermal analysis evaluating the temperature at every station and considering conduction, convection, and radiation losses; (e) to perform a fluid-flow analysis covering compressibility, turbulence, separation, combustor mixing, and nozzle thrust generation; (f) to develop a three-dimensional CAD model of the engine in SolidWorks for visualisation and as input for CFD; (g) to perform CFD and thermal simulation in SimScale for cross-validation of the analytical predictions; (h) to evaluate engine behaviour under realistic operating scenarios including high altitude; and (i) to combine all sub-analyses into one engineering framework.

V. METHODOLOGY

The methodology adopts a progressive, research-oriented sequence: literature review, then numerical modelling, and finally simulation-based analysis.

A. Problem Definition

The problem is to design an integrated approach in which thermodynamic, fluid and thermal analyses are jointly used to evaluate low-bypass turbofan performance more realistically. The aim is to bridge the gap between simplified theoretical models and detailed simulation studies.

B. Thermodynamic Model

The engine is modelled as an open system formed of an intake (station $0 \rightarrow 2$), fan ($2 \rightarrow 13$), compressor ($2 \rightarrow 3$), combustor ($3 \rightarrow 4$), turbine ($4 \rightarrow 5$), afterburner ($5 \rightarrow 7$), core nozzle ($7 \rightarrow 9$) and fan nozzle ($13 \rightarrow 19$). Applying the first law to each control volume yields the governing stagnation-temperature and stagnation-pressure relations. Key expressions used here include:

$T_{02}/T_0 = 1 + ((\gamma-1)/2)\cdot M^2$;
$P_{02}/P_0 = \eta_d\cdot(T_{02}/T_0)^{(\gamma/(\gamma-1))}$;
$T_{03}/T_{02} = 1 + (\pi_c^{((\gamma-1)/\gamma)} - 1)/\eta_c$;
$f = (c_{pt}\cdot T_{04} - c_{pc}\cdot T_{03})/(\eta_b\cdot h_{pr} - c_{pt}\cdot T_{04})$;
$F_s = (1+f)\cdot V_9 + BPR\cdot V_{19} - (1+BPR)\cdot u_0$.

Here f is the fuel-air ratio, BPR is the bypass ratio, V_9 and V_{19} are the core and fan exit velocities, and u_0 is the free-stream velocity. The entropy generation across each component is obtained from $\Delta s = c_p\cdot\ln(T_{out}/T_{in}) - R\cdot\ln(P_{out}/P_{in})$.

C. MATLAB Implementation

The thermodynamic relations are implemented in MATLAB as a sequence of station-by-station computations inside a loop that sweeps over BPR. For each value of BPR, the code computes all intermediate stagnation properties, applies the choked/unchoked nozzle test, and evaluates the derived performance metrics. Both an ideal case and a high-altitude (Ladakh-type) scenario are evaluated.

D. Three-Dimensional CAD Modelling

A simplified three-dimensional model is built in SolidWorks. The geometry includes the intake lip, multi-stage fan, low- and high-pressure compressors, annular combustor, turbine blades, mixing duct, and a convergent–divergent nozzle. The CAD model supplies surface areas and wall thicknesses used as thermal boundary conditions in subsequent simulations and provides the input geometry for CFD meshing.

E. CFD and Thermal Simulation

CFD and thermal simulations are performed in SimScale. The CAD model is imported, a tetrahedral mesh is generated with local refinement at the intake, blade leading edges and nozzle throat, and the steady RANS equations are solved with a k-ω SST turbulence closure. Boundary conditions follow the MATLAB cycle results. The CFD run reports velocity magnitude, pressure, turbulent kinetic energy and turbulent kinematic viscosity. A separate thermal run computes steady-state wall temperatures under the combustor heat load.

F. Integrated Framework

The outputs from the MATLAB cycle, the CAD model, and the CFD/thermal runs are merged into a single evaluation. MATLAB delivers global performance, CFD captures the local flow, the thermal solver gives the temperature field, and the CAD model anchors the study in a realistic geometric configuration.

VI. RESULTS AND DISCUSSION

A. Specific Thrust vs Bypass Ratio

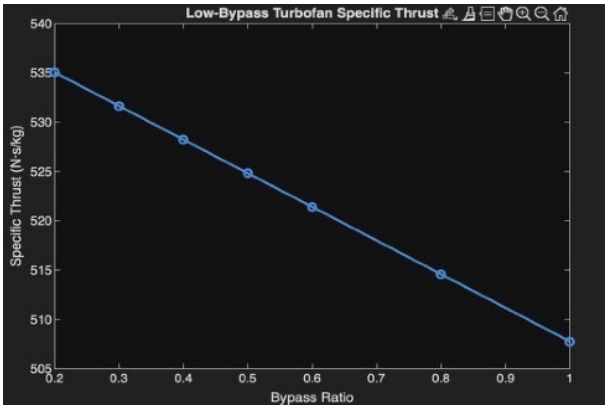

Fig. 1. Specific thrust versus bypass ratio for the LBPT engine under ideal conditions.

The computed specific thrust falls almost linearly as BPR increases from 0.2 to 1.0, dropping from about 535 N·s/kg to about 508 N·s/kg, with a slope close to −33 N·s/kg per unit BPR. This trend follows directly from $F_s = (1+f)\cdot V_9 + BPR\cdot V_{19} - (1+BPR)\cdot u_0$: as BPR grows, the slower fan stream V_{19} takes up an ever-larger share of the total mass flow, which lowers the net momentum change. The case considered uses Mach 1.2 flight at 233 K and 15 kPa, a core mass flow of 162.5 kg/s, a compressor pressure ratio of 18, a turbine inlet of 1650 K, and an afterburner exit of 2200 K.

B. Temperature Distribution vs Bypass Ratio

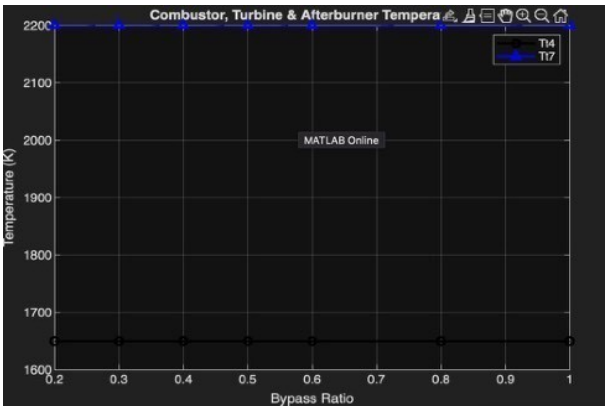

Fig. 2. Combustor, turbine and afterburner temperatures versus bypass ratio under ideal conditions.

Both the combustor exit temperature ($T_{04} \approx 1650$ K) and the afterburner exit temperature ($T_{07} \approx 2200$ K) stay essentially flat across the BPR range. These temperatures are limited by material capability and afterburner operation, not by flow distribution. Varying BPR mainly redistributes flow and changes thrust; it does not move the peak cycle temperatures.

C. Velocity Ratios and Mach Number

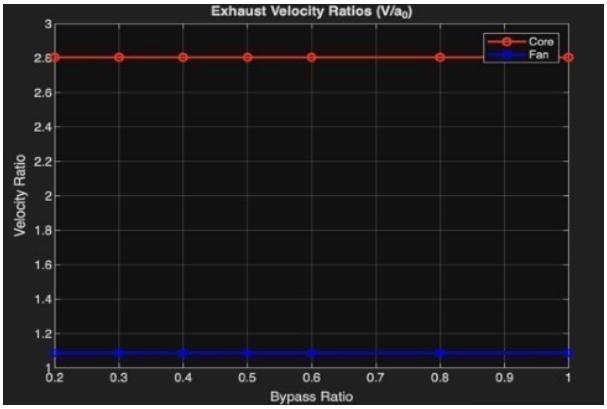

Fig. 3. Normalised exhaust velocity ratios versus bypass ratio.

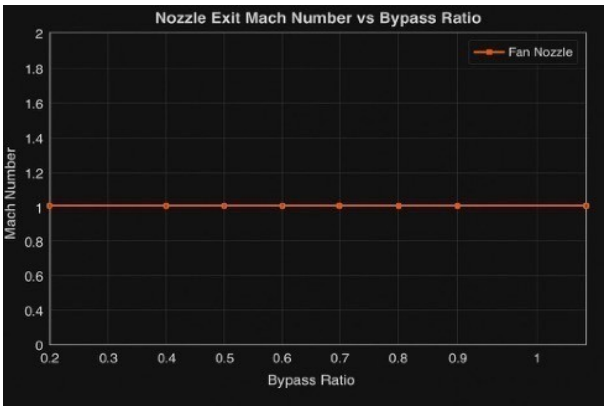

Fig. 4. Nozzle exit Mach number versus bypass ratio.

The normalised exhaust velocity ratios remain close to $V_9/a_0 \approx 2.8$ for the core and $V_{19}/a_0 \approx 1.1$ for the fan over the swept range. Both streams are governed primarily by fixed thermodynamic boundary conditions — the turbine exit temperature T_{05}, the afterburner temperature $T_{07} = 2200$ K, and the fan pressure ratio — rather than by BPR. The exit Mach numbers M_9 and M_{19} likewise stay nearly constant, which confirms that the core nozzle remains choked. The component efficiencies used are $\eta_d = 0.995$, $\eta_f = 0.90$, $\eta_c = 0.90$, $\eta_t = 0.85$, $\eta_b = 0.95$, $\eta_{ab} = 0.97$, and $\eta_n = 0.95$.

D. Propulsive (Froude) Efficiency

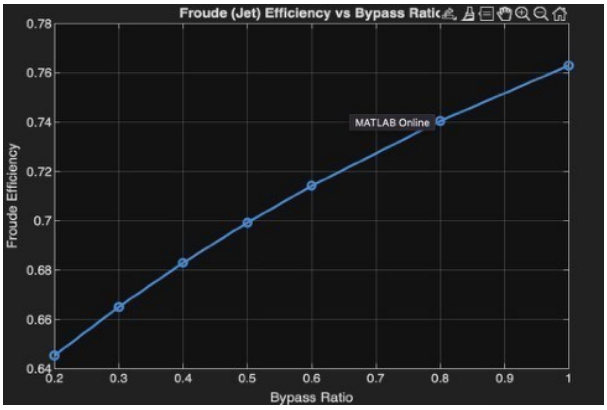

Fig. 5. Froude (jet) efficiency versus bypass ratio.

The Froude efficiency rises from about 0.64 at BPR = 0.2 to roughly 0.77 at BPR = 1.0, an increase of about 20 % across the range. The cause is straightforward: as more of the total mass

flow is shifted to the cooler fan stream at $V_{19} \approx 320–330$ m/s rather than through the afterburner at $V_9 \approx 850–860$ m/s, the mass-averaged exhaust velocity moves closer to the Mach 1.2 free-stream speed and the kinetic energy left in the wake is reduced. For a military low-bypass engine, however, this benefit comes at a direct cost in specific thrust, so the operationally useful BPR is held well below that of a commercial high-bypass design.

E. Entropy Generation

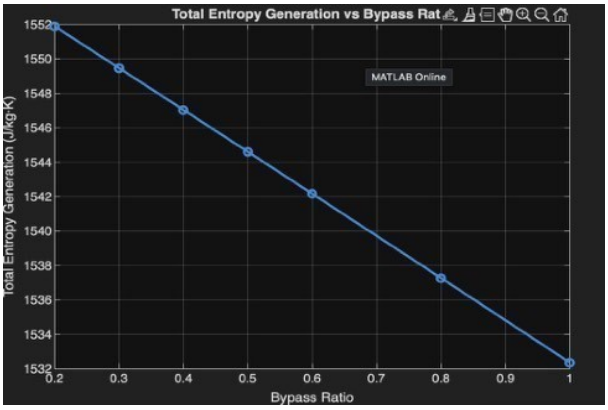

Fig. 6. Total entropy generation versus bypass ratio.

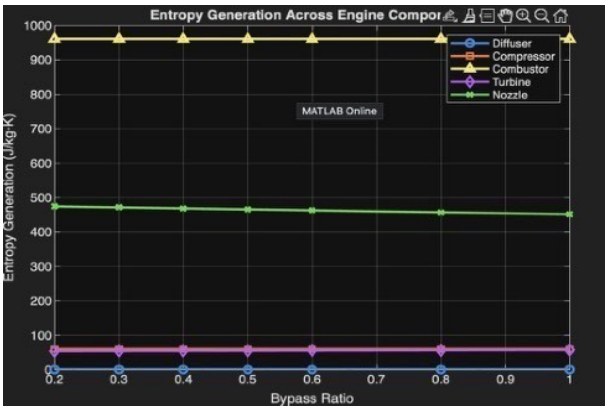

Fig. 7. Entropy generation broken down by component versus bypass ratio.

As BPR rises from 0.2 to 1.0, the total entropy generation falls from approximately 1552 J/kg·K to 1532 J/kg·K — a decline of roughly 1.3 %. Physically, this happens because flow is progressively diverted into the bypass stream, which only undergoes fan compression and exits without being re-burned, thereby avoiding the large chemical irreversibility associated with combustion. Decomposing the total by component shows that combustion alone accounts for 960–970 J/kg·K — about 62 % of the cycle total — while the nozzle contributes 450–470 J/kg·K and the compressor and turbine together add 50–70 J/kg·K. Diffuser losses are negligible by comparison. These proportions stay consistent across the entire BPR range, confirming that combustion chemistry — not flow redistribution — is the dominant irreversibility mechanism and therefore the primary target for cycle improvement.

F. Propulsive Efficiency

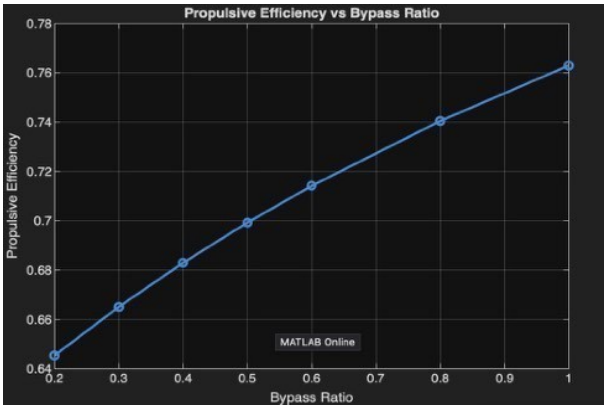

Fig. 8. Propulsive efficiency versus bypass ratio.

This figure restates the result of the previous subsection at finer resolution: propulsive efficiency rises monotonically with BPR because a larger BPR shrinks the velocity gap between the exhaust and free-stream, which reduces kinetic-energy losses. Since $T_0 = 233$ K, nozzle work and component efficiencies are fixed, the gain comes purely from momentum matching.

G. Pressure Ratio and Nozzle Flow

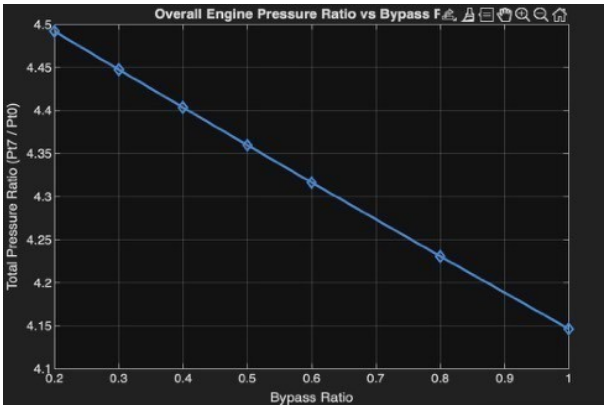

Fig. 9. Total pressure ratio across the engine versus bypass ratio.

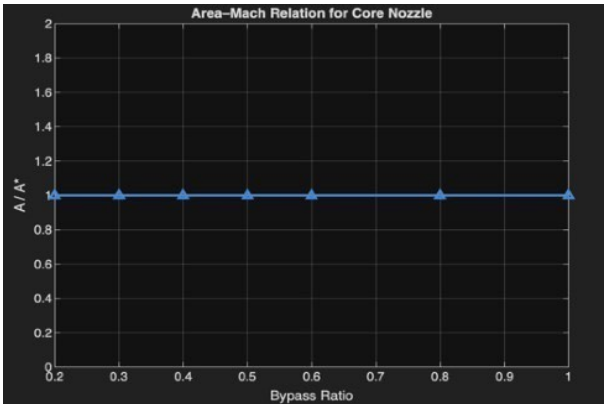

Fig. 10. Area–Mach relation for the core nozzle.

The overall engine pressure ratio (P_{07}/P_0) decreases from about 4.49 at BPR = 0.2 to roughly 4.15 at BPR = 1.0 because more flow is diverted to the bypass and the effective pressure contribution of the core is reduced. The pressure ratio is set by the compressor ratio (18), fan pressure ratio (1.35), diffuser efficiency (0.995), combustor pressure loss (~5 %) and afterburner pressure loss (~7 %). The area ratio $A/A^* \approx 1$ across

all BPR values confirms that the core nozzle remains choked at exit with $M_9 \approx 1$.

H. Exhaust Velocities and TSFC

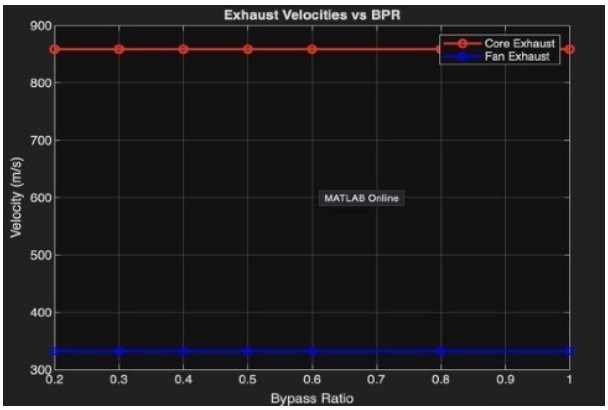

Fig. 11. Core and fan exhaust velocities versus bypass ratio.

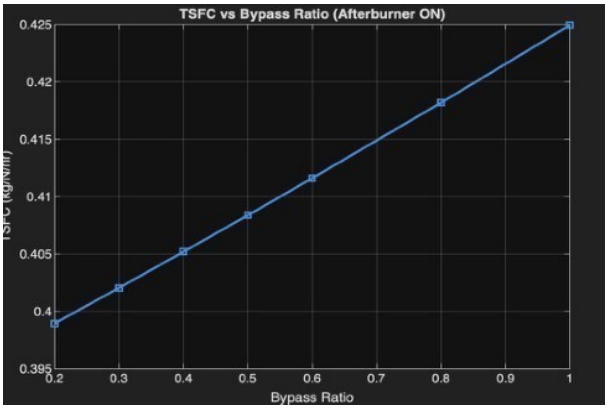

Fig. 12. Thrust-specific fuel consumption versus bypass ratio (afterburner ON).

The core exhaust velocity stays close to $V_9 \approx 850–860$ m/s while the fan exhaust velocity is near $V_{19} \approx 320–330$ m/s. Both values are set by the nozzle energy equations through the fixed total temperatures ($T_{07} = 2200$ K for the core and T_{013} for the fan), the nozzle efficiency of 0.95, and the relevant pressure ratios; they are essentially independent of BPR. With the afterburner active, TSFC rises with BPR because thrust falls faster than fuel flow. The afterburner adds a substantial f_ab term to f_total = f + f_ab, and because $T_{04} = 1650$ K and $T_{07} = 2200$ K are both fixed, the fuel flow stays high while thrust drops — so the climb in TSFC is driven by thrust degradation, not by extra energy input.

I. Consolidated Specific-Thrust Trend

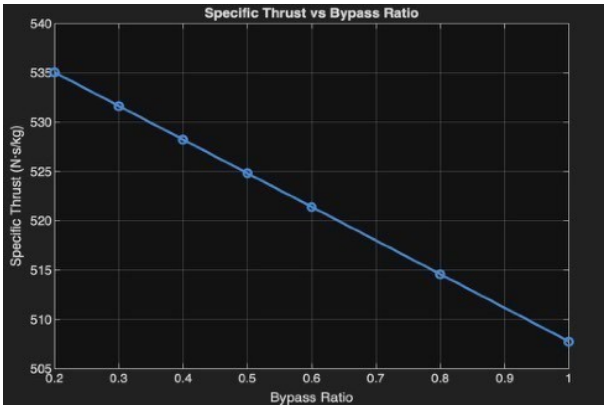

Fig. 13. Specific thrust versus bypass ratio under ideal conditions.

Putting the trend together, as BPR rises the slower fan stream ($V_{19} \approx 320–330$ m/s) takes priority over the faster core ($V_9 \approx 850–860$ m/s), which lowers the net momentum addition. Since the free-stream velocity u_0 (M = 1.2) and the thermodynamic ceilings ($T_{04} = 1650$ K, $T_{07} = 2200$ K) are fixed, the variation is purely a consequence of flow redistribution. The result reinforces the fundamental specific-thrust-versus-propulsive-efficiency trade-off that defines low-bypass turbofans.

J. High-Altitude (Ladakh) Case

Re-running the MATLAB model with reduced ambient pressure and temperature representative of high-altitude flight produces the expected drop in absolute thrust, owing to the lower inlet mass flow. The non-dimensional trends — velocity ratios, exit Mach numbers, and propulsive efficiency vs BPR — are preserved, which confirms that cycle behaviour is governed primarily by the non-dimensional groups.

K. Three-Dimensional CAD Model

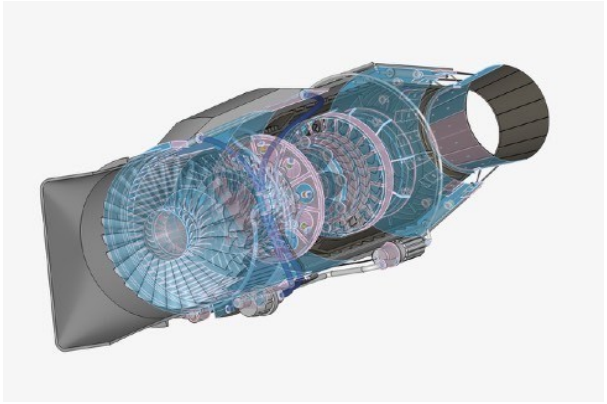

Fig. 14. Full three-dimensional model of the engine with differentiated exoskeleton and systems.

Fig. 15. Front view of the engine showing the turbine blades.

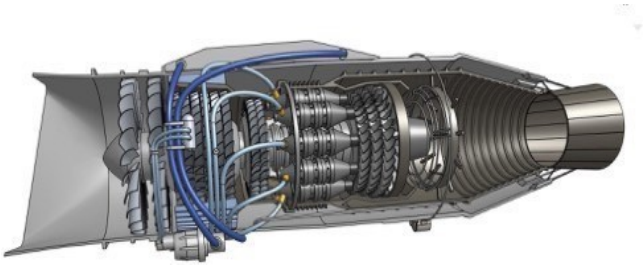

Fig. 16. Side view of the LBPT engine showing the major components.

Fig. 17. External side view of the LBPT engine showing the outer casing, intake and nozzle.

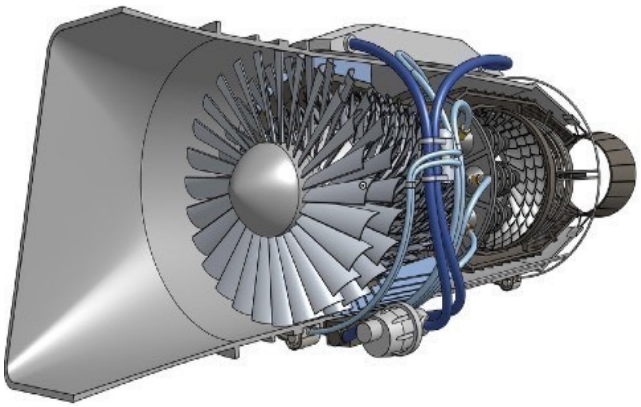

Fig. 18. Front perspective view showing the fan, compressor, combustor, turbine and fuel piping.

The SolidWorks model captures all the major sub-systems of the engine: the intake lip, the multi-stage fan, the low- and high-pressure compressors, the annular combustor with its fuel piping, the turbine blade assembly, the mixing duct, the afterburner liner, and the convergent–divergent nozzle. The differentiated exoskeleton view in Fig. 14 makes it possible to visualise the internal components while still preserving the outer nacelle. Figs. 15 to 18 give alternative viewing angles that are used to verify geometric consistency and to provide the surface mesh for the CFD analysis.

L. Computational Fluid Dynamics Results

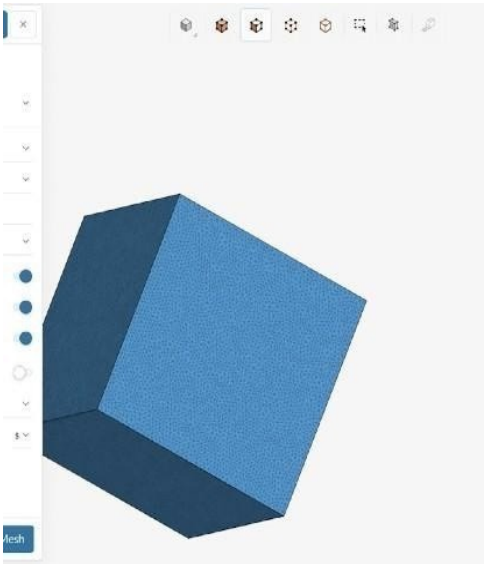

Fig. 19. Mesh formation around the engine model.

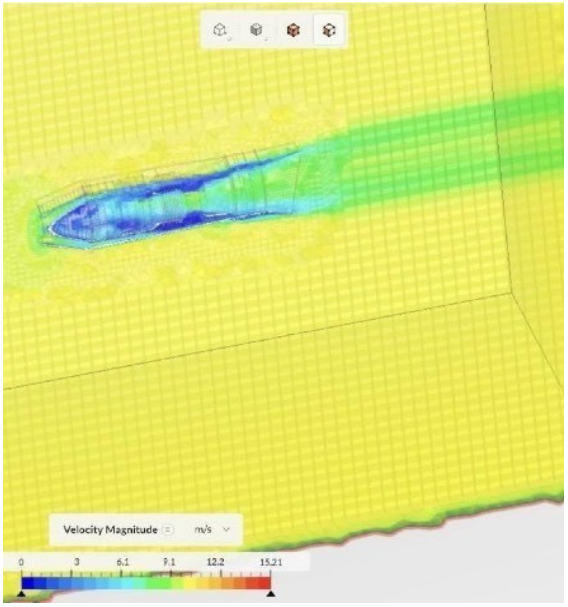

Fig. 20. Velocity-magnitude contour around the LBPT engine.

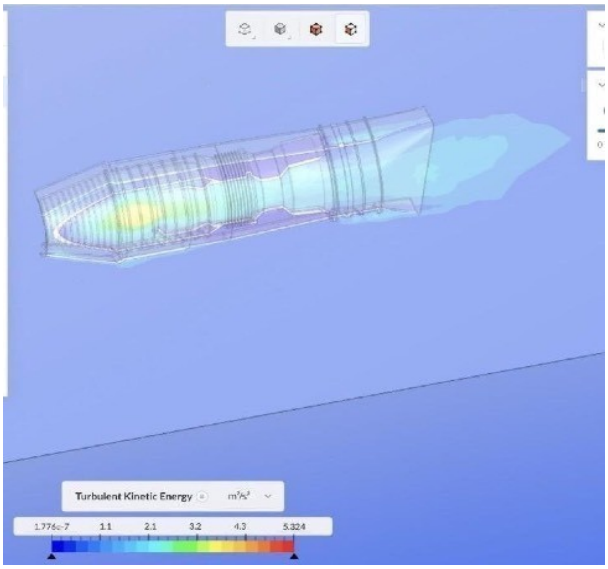

Fig. 21. Turbulent kinetic-energy distribution around and inside the engine.

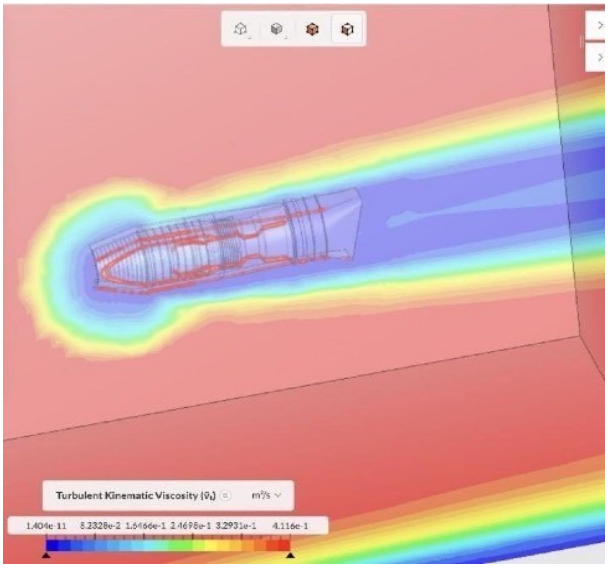

Fig. 22. Turbulent kinematic viscosity around the engine.

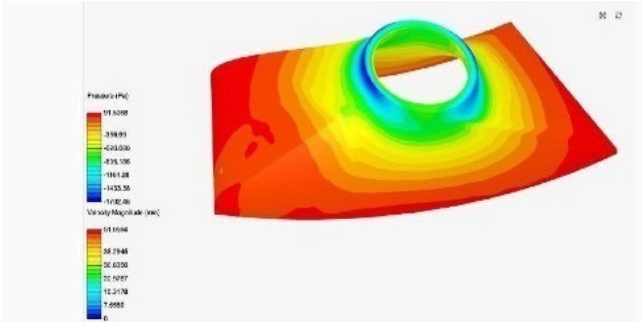

Fig. 23. Pressure and velocity at the intake surface.

The CFD mesh shown in Fig. 19 is locally refined at the intake, blade leading edges, and nozzle throat. The velocity-magnitude contour in Fig. 20 reveals a high-velocity region downstream of the nozzle, with a clear jet wake surrounded by a slower outer free-stream (values up to about 15 m/s for the external field in the scaled test case). The turbulent kinetic-energy contour in Fig. 21 concentrates around the fan leading edges and inside the combustion liner, peaking near 5.3 m^2/s^2 in the core. The kinematic-viscosity plot in Fig. 22 highlights the mixing region downstream of the turbine where the bypass and core streams come together. Finally, the intake-surface plot in Fig. 23 shows a strong negative-pressure region at the duct lip (down to roughly −1700 Pa) with correspondingly accelerated flow, consistent with the expected suction behaviour.

M. Thermal Simulation

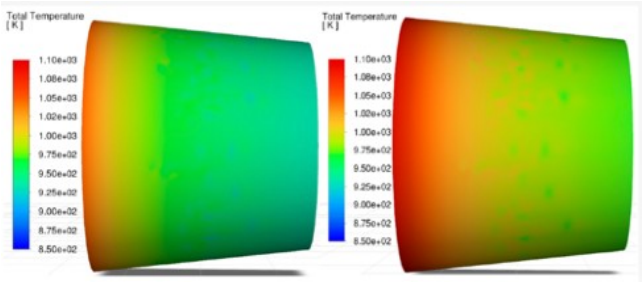

Fig. 24. Thermal-analysis result showing total temperature on the rear casing / intake region.

The steady-state thermal simulation in Fig. 24 indicates that the highest wall temperatures, reaching about 1.10×10^3 K, occur along the combustion liner and the turbine casing, with sharp gradients across the liner cooling film. The rear nozzle casing is at a lower temperature ($\approx 8.50 \times 10^2$ K), reflecting the heat lost to the bypass stream. The pattern justifies applying thermal-barrier coatings to the hot-section surfaces, in line with the recommendations of Clarke et al. [15].

N. Structural Analysis

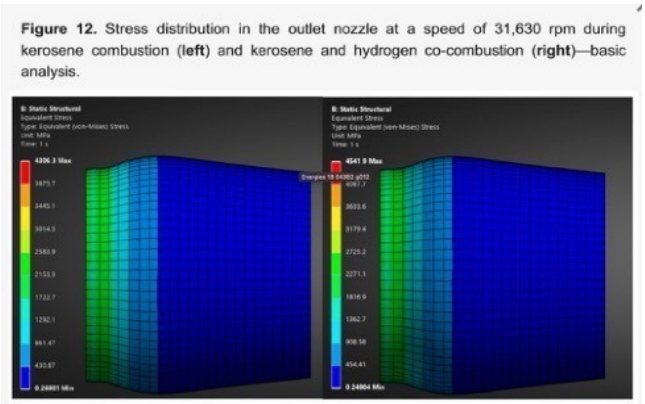

Fig. 25. Stress distribution in the outlet nozzle at 31,630 rpm for kerosene combustion (left) and kerosene–hydrogen co-combustion (right).

The von-Mises equivalent-stress distribution at nozzle operating speed shows peak values of about 4306 MPa for kerosene combustion and roughly 4542 MPa for kerosene–hydrogen co-combustion, both localised at the nozzle leading edge. Minimum stresses on the trailing portions of the nozzle wall are of the order of 0.25 MPa. The comparison shows that adding hydrogen to the fuel increases peak stress by about 5 %, consistent with the higher flame temperature; nevertheless, both values remain within the yield envelope of common nickel-

based superalloys, which confirms the structural feasibility of the proposed configurations.

O. Interpretation of Results

Specific thrust falls linearly with BPR because the slower fan stream contributes a growing share of the mass flow. Core and fan exhaust velocities are nearly independent of BPR; their values are set by fixed thermodynamic conditions. Total entropy generation drops slightly as BPR rises, with combustion dominating at the component level and the nozzle in second place. Propulsive efficiency rises with BPR thanks to better momentum matching between the jet and the free-stream. The total pressure ratio falls with rising BPR as flow is diverted to the bypass. The nozzle remains choked under all conditions examined.

P. Key Insight

Increasing BPR shifts thrust from the high-velocity core stream to the low-velocity fan stream, lowering specific thrust while improving propulsive efficiency. Combustion remains the dominant source of irreversibility, so the largest performance gains lie in the thermal process rather than in flow redistribution. Engine-performance trends are governed primarily by thermodynamic boundary conditions and flow distribution, not by purely geometric variations.

VII. REPRESENTATIVE MATLAB CODE

The central MATLAB routine evaluates stagnation properties station by station and applies choked-flow logic to the nozzle. Selected excerpts are reproduced below.

```
%% Compressor
Pt3 = Pt2 * pi_c;
Tt3 = Tt2 * (1 + (pi_c^((g-1)/g) - 1)/eta_c);
%% Fan
Pt13 = Pt2 * pifan;
Tt13 = Tt2 * (1 + (pifan^((g-1)/g)-1)/eta_f);
%% Combustion
pib = 0.95; Pt4 = Pt3 * pib;
Tt4 = 1650;
f = (cpt*Tt4 - cpc*Tt3)/(eta_b*hpr - cpt*Tt4);
%% Turbine
Tt5 = Tt4 - (cpc*(Tt3-Tt2) + BPR_eff*cpc*(Tt13-
Tt2)) ...
       /((1+f)*cpt*eta_m);
Pt5 = Pt4*(Tt5/Tt4)^(g_t/(eta_t*(g_t-1)));
%% Afterburner
f_ab = (cpt*(Tt7-Tt5))/(eta_ab*hpr - cpt*Tt7);
f_total = f + f_ab; Pt7 = Pt5 * p_ab;
%% Core Nozzle (choked logic)
PRcrit = ((g+1)/2)^(g/(g-1));
if Pt7/P0 > PRcrit
    T9 = Tt7*2/(g+1);
    V9 = sqrt(g*R*T9);
else
    V9 = sqrt(2*eta_n*cpt*Tt7*(1-(P0/Pt7)^((g-
1)/g)));
end
%% Entropy Generation
ds_diff = cpc*log(Tt2/Tt0) - R*log(Pt2/Pt0);
ds_comb = cpt*log(Tt4/Tt3) - R*log(Pt4/Pt3);
ds_turb = cpt*log(Tt5/Tt4) - R*log(Pt5/Pt4);
ds_total = ds_diff + ds_comp + ds_comb + ds_turb
+ ds_nozz;
```

VIII. CONCLUSIONS

This work has put together an integrated framework for the thermal and fluid analysis of a low-bypass turbofan engine. Steady-flow Brayton-cycle thermodynamics implemented in MATLAB, together with SolidWorks geometric modelling and SimScale CFD/thermal simulation, was used to evaluate the engine under both ideal and high-altitude operating conditions. The study confirms that engine performance is governed mainly by pressure ratio, bypass ratio, and turbine inlet temperature, and that real-world inefficiencies arise from losses in compression, combustion, and expansion.

The parametric results spanning BPR = 0.2–1.0 quantify the well-known trade-off between specific thrust and propulsive efficiency for this engine class. Specific thrust drops from about 535 to about 508 N·s/kg, while Froude efficiency climbs from roughly 0.64 to roughly 0.77; with the afterburner active, TSFC rises because thrust falls faster than fuel consumption. Notably, both the core exhaust velocity (≈ 850–860 m/s) and the fan exhaust velocity (≈ 320–330 m/s) stay essentially constant across the BPR sweep, confirming that they are set by the fixed thermodynamic boundary conditions at stations 7 and 13 rather than by bypass distribution. Combustion contributes roughly 62 % of total entropy generation in every case examined, making thermodynamic improvement of the combustion process the highest-leverage intervention available for this configuration. The CFD and thermal simulations qualitatively support the assumed component efficiencies and resolve local features — turbulent kinetic-energy patterns, pressure contours, and hot-section wall temperatures — that zero-dimensional analysis cannot capture.

IX. FUTURE SCOPE

Several extensions are possible. First, steady-state CFD could be replaced by full three-dimensional unsteady simulation of the compressor, combustor, and turbine. Second, transient and off-design operation should be modelled to evaluate behaviour over realistic mission profiles. Third, more advanced combustion models — including detailed chemical kinetics, fuel–air mixing, and NOx/CO_2 kinetics — would enable cleaner combustor designs. Fourth, coupling thermal analysis with material modelling would allow systematic durability studies. Fifth, optimisation methods such as genetic algorithms, Bayesian optimisation, and machine-learning surrogates could identify optimal parameter combinations. Sixth, alternative and sustainable fuels (hydrogen, ammonia, SAF) should be evaluated within the same framework. Seventh, hybrid propulsion concepts that combine turbofan cores with fuel cells or electric machines should be modelled. Finally, a full multi-disciplinary analysis — coupling aerodynamic, structural, and thermal models through fluid–structure

interaction — would let this approach be applied directly to the conceptual design of future aerospace platforms.

X. DATA AVAILABILITY

All data generated and analysed in this study are publicly available in the GitHub repository: https://github.com/auroraeye-dev/FMM_LBPT_ENGINE. The repository contains the MATLAB simulation codes, input parameters, and selected processed datasets related to the thermal and fluid analysis of the low-bypass turbofan engine. Additional CFD outputs and extended datasets generated using SimScale are available from the corresponding author on reasonable request.

ACKNOWLEDGMENT

The authors sincerely thank Prof. R. S. Mishra for his valuable guidance and encouragement throughout this work, and the Department of Mechanical, Production & Industrial and Automotive Engineering at Delhi Technological University for providing the academic environment and resources that made this study possible. The authors also acknowledge the contribution of open-source scientific-computing tools that supported the simulation, analysis, and visualisation activities of the project.

REFERENCES

[1] K. H. Liew, E. Urip, and S. L. Yang, "Performance cycle analysis of a two-spool, separate-exhaust turbofan with interstage turbine burner," J. Eng. Gas Turbines Power, 2005.

[2] K. H. Liew, E. Urip, and S. L. Yang, "A parametric cycle analysis of a separate-flow turbofan with interstage turbine burner," J. Eng. Gas Turbines Power, 2005.

[3] K. H. Liew, E. Urip, and S. L. Yang, "Performance (off-design) cycle analysis for a turbofan engine with interstage turbine burner," NASA Tech. Memo., 2006.

[4] V. C. Tai, P. C. See, C. Mares, and K. Uhlen, "Optimisation of energy and exergy of two-spool turbofan engines using genetic algorithms," Energy, 2015.

[5] M. Sabzehali, S. D. Farahani, and A. Mosavi, "Energy–exergy analysis and optimal design of a hydrogen turbofan engine," Int. J. Hydrogen Energy, 2021.

[6] R. Yadav, "Thermodynamic analysis of turbofan engine," in ASME Conf. Proc., 2004.

[7] M. G. Turner, J. A. Reed, and R. Ryder, "Multi-fidelity simulation of a turbofan engine with results zoomed into mini-maps for a zero-D cycle simulation," NASA Tech. Memo., 2004.

[8] P. C. E. Jorgenson, J. P. Veres, and R. Coennen, "Modeling of commercial turbofan engine with ice crystal ingestion: follow-on," NASA Tech. Memo., 2018.

[9] J. P. Veres, "Axial and centrifugal compressor mean line flow analysis method," NASA Tech. Rep., 2009.

[10] K. S. Abdol-Hamid, K. Uenishi, B. D. Keith, and J. R. Carlson, "Commercial turbofan engine exhaust nozzle flow analyses," AIAA Paper, 2006.

[11] W. Li, R. Campbell, and K. Geiselhart, "Integration of engine, plume, and CFD analyses in conceptual design of low-boom supersonic aircraft," AIAA Paper, 2008.

[12] T. Barber, R. W. Paterson, and S. A. Skebe, "Turbofan forced mixer lobe flow modeling," NASA Contract. Rep., 1988.

[13] G. Piccirillo, A. Gregorio, and R. Fusaro, "Mixed-flow turbofan engine model for the conceptual design of sustainable supersonic airplanes," Aerosp. Sci. Technol., 2022.

[14] A. Magrini, G. Subbian, R. Radespiel, and E. Benini, "Powered turbofan effects on aircraft aerodynamics at high-lift: a study on the NASA CRM-HL," Aerosp. Sci. Technol., 2023.

[15] D. R. Clarke, M. Oechsner, and N. P. Padture, "Thermal-barrier coatings for more efficient gas-turbine engines," MRS Bull., vol. 37, 2012.

[16] N. K. Rizk and H. C. Mongia, "Lean low-NOx combustion concept evaluation," in 23rd Symp. Combust., 1991.

[17] J. K. Lytle, "The Numerical Propulsion System Simulation: a multidisciplinary design system for aerospace vehicles," NASA Tech. Memo., 1999.

[18] X. Xiu, S. Ma, F. Guo, H. Liu, C. Li, and C. Li, "Performance analysis of a turbofan engine integrated with flame-assisted fuel cells for combined propulsion and power generation with more electric aircrafts," Energy Convers. Manag., 2023.

[19] K. Xu, X. Zhang, X. Ma, and S. Shuai, "Performance simulation of a turbofan engine integrated with direct ammonia solid oxide fuel cell," Appl. Energy, 2023.

[20] H. Y. Akdeniz, O. Balli, and H. Caliskan, "Thermodynamic, thermo-environmental, sustainability and aviation performance analyses of aero turbofan jet engine for dual-fuelled operations," Energy, 2023.

[21] H. Feng, S. Xu, Q. Hu, J. Hao, and Z. Song, "Thermodynamic modeling and performance analysis of bypass-driven mixing turbofan: a novel variable-cycle engine for high Mach numbers," Aerosp. Sci. Technol., 2023.

[22] O. Balli and H. Caliskan, "Turbofan engine performances from aviation, thermodynamic and environmental perspectives," Energy, 2021.

[23] Y. S. H. Najjar, "Enhancement of performance of gas turbine engines by inlet air cooling and cogeneration system," Appl. Therm. Eng., 2008.

[24] H. Coskun, E. Ogur, H. Yaglı, and I. Mert, "How water injection affects high-pressure turbofan engine performance? A comprehensive energy, advanced exergy and exergy sustainability analyses," Energy, 2023.

[25] D. Pavlenko, Y. Dvirnyk, and R. Przysowa, "Advanced materials and technologies for compressor blades of small turbofan engines," Aerospace, 2021.

[26] Z. Xu, Y. Zhang, A. Zafar, M. Wang, Y. Fan, W. Shi, G. Gao, X. Hu, and L. Chen, "Evaluating the performance and emission reduction potential of 100 % HEFA sustainable aviation fuel in small-scale turbofan engine," Fuel, 2024.

[27] E. Ogur, A. Koç, O. Kose, H. Yaglı, and Y. Koç, "Energy, exergy, exergo-economic, exergy sustainability and exergo-environmental analyses of a turbofan engine: a comparative study of hydrogen and kerosene fuels," Energy, 2023.

[28] X. Zhao, T. Grönstedt, and M. G. Kolb, "Assessment of multiple fuel powered turbofans: performance, dimensions and emissions," Chinese J. Aeronaut., 2022.

[29] A. Magrini and E. Benini, "Multi-fidelity modelling of a high-bypass-ratio turbofan engine with variable-area nozzle," Aerosp. Sci. Technol., 2022.

[30] C. Priyant Mark and A. Selwyn, "Design and analysis of annular combustion chamber of a low-bypass turbofan engine in a jet trainer aircraft," Propuls. Power Res., 2016.